JOURNAL OF MATERIALS SCIENCE 30 (1995) 2438–2445

Failure mechanics in ternary composites of polypropylene with inorganic fillers and elastomer inclusions

Part II *Fracture toughness*

J. JANCAR, A. T. DIBENEDETTO
Institute of Materials Science, University of Connecticut, 97 North Eagleville Road, Storrs, CT 06269, USA

The effects of phase morphology, interfacial adhesion and filler particle shape and volume fraction on the fracture toughness of polypropylene (PP) filled with $CaCO_3$ or $Mg(OH)_2$ and ethylene–propylene elastomer (EPR) were investigated. Separation of the inorganic filler and elastomer particles was achieved using maleic-anhydride-grafted PP (MPP) to enhance the inorganic filler–matrix adhesion. Encapsulation of the rigid filler by the elastomer was achieved by using maleic-anhydride-grafted EPR (MEPR) to increase the inorganic filler–elastomer adhesion. The two limiting morphologies differed significantly in fracture toughness under impact loading at the same material composition. A model for a mixed mode of failure, accounting for the plane strain and plane stress contributions to the strain energy release rate, G_c, was used to predict the upper and lower limits for G_c for the two limiting morphologies over an interval of elastomer volume fractions, v_e, from 0–0.2 at a constant filler volume fraction, $V_f = 0.3$, and over the filler volume fraction from 0–0.4 at constant EPR content. The role of material yield strength in controlling fracture toughness has been described successfully using Irwin's analysis of plastic zone size. The presence of elastomer enhances both the critical strain energy release rate for crack initiation, G_c, and the resistance to crack propagation as expressed by Charpy notched impact strength for the two limiting morphologies. Satisfactory agreement was found between the experimental data and predictions of upper and lower G_c limits.

1. Introduction

One of the shortcomings most adversely affecting the utilization of polypropylene (PP) filled with flame-retardant magnesium hydroxide ($Mg(OH)_2$) is the steep reduction of subambient fracture toughness compared to that of neat PP. Generally, an increase in the resistance to crack initiation and growth can be achieved by modifying the stress state within the specimen, altering the size of the crack-tip plastic zone and inducing favourable mechanisms of matrix failure [1–11]. The most common method of obtaining all of these changes is to "rubber toughen" the matrix phase by the addition of elastomer inclusions. Under proper processing conditions the presence of elastomer particles will reduce the matrix yield strength, thereby increasing the size of crack-tip plastic zone and producing changes in PP morphology.

Unlike the case of toughening binary blends, where the primary variables controlling the fracture resistance are elastomer volume fraction and the size and distribution of elastomer inclusions, the toughness of ternary blends is extremely sensitive to the relative spatial arrangement of elastomer and filler inclusions [12–14]. As was shown in previous publications [15, 16], when adhesion between the PP and rigid filler is enhanced by the addition of maleic anhydride (MAH) to the PP, the elastomer and rigid filler are separately dispersed in the matrix phase and the ternary composite acts, under equivalent loading, similarly to that of a binary PP/elastomer blend [11], reducing the composite yield strength and elastic modulus while increasing the strain at break [17]. A lower limit of strain energy release rate G_c (or fracture toughness, K_c) for these materials can be calculated using linear elastic fracture mechanics (LEFM) and Irwin's concept of the plastic zone [18] along with knowledge of the yield strength [10, 11].

When adhesion between the elastomer phase and rigid filler is enhanced by addition of MAH to the elastomer, the filler becomes encapsulated by the elastomer, promoting the formation of core–shell inclusions. The change in morphology modifies the character of the stress field in the vicinity of heterogeneities, thereby changing the main failure mechanism from unstable localized shear bonding nucleated at the filler surface, to delocalized shear yielding. As was shown earlier, LEFM and Irwin's concept of plastic zone, along with the Nicolais–Narkis model for yield

0022–2461

strength of these materials can be utilized to predict an upper limit of G_c (or K_c).

The aim of the present work was to use current models for the composite yield strength and the concept of mixed mode of fracture to predict upper and lower limits of critical strain energy release rate, G_c, for the two limiting morphologies, i.e., complete separation of the rigid filler and elastomer inclusions and complete encapsulation of the filler by the elastomer. Additionally, in order to assess the effects of different structural variables on the standardized impact strength, the effects of the same variables on the Charpy notched impact strength, CNIS, were investigated.

2. Experimental procedure

Commercial polypropylene Mosten 58.412 (Litvinov Chemical Works, Czech Republic), melt flow ratio of 4 g/10 min (230 °C, 21.6 N), was used as a matrix. Maleated PP (Research Institute of Macromolecular Chemistry (RIMC), Brno, Czech Republic), melt flow ratio 20 g/10 min (230 °C, 21.6 N) and containing 2 wt % grafted maleic anhydride, was used to modify matrix–filler adhesion. PP and maleated PP (MPP) were mixed in a PLO 651 Brabender Plasticorder (190 °C, 50 r.p.m., 10 min) to achieve the required concentration of carboxyl groups in the matrix.

Ethylene–propylene random copolymer (EPR) Dutral CO 054 (Himont, Italy), $T_g = -57$ °C, $M_w = 180\,000$, was used as an elastomer. A maleated version of Dutral CO 054 (RIMC, Brno, Czech Republic), containing 2 wt % grafted MAH, was mixed with EPR to achieve the required concentration of carboxyl groups in the elastomer under the same conditions as described above.

Two batches of platelet-shaped $Mg(OH)_2$ filler of the same average aspect ratio of 5 and specific surface area of 7 and 18 $m^2 g^{-1}$, respectively (RIMC, Brno, Czech Republic) were used as flame-retardant fillers. Additionally, irregularly shaped $CaCO_3$ filler, Durcal 2 (Omya, Switzerland), with average particle diameter of 3.6 μm and specific surface area of 2.5 $m^2 g^{-1}$ was used to investigate the effect of particle shape. Only untreated fillers were used to avoid the effects of commonly utilized low molar weight surface treatments.

PP/filler/elastomer composites were prepared mixing all the components in a one step procedure (PLO 651 Brabender Plasticorder, 200 °C, 50 r.p.m., 10 min). Rectangular specimens were cut from the compression-moulded sheets (200 °C for 4 min at atmospheric pressure, 2 min under 6 MPa, cooled down under pressure at an average cooling rate of 20 °C min^{-1}). Strain energy release rate, G_c, and Charpy notched impact strength, CNIS, were measured using a Zwick impact pendulum (impact speed of 2.6 m s^{-1}) and CEAST instrumented impact tester (impact speed of 3.6 m s^{-1}), respectively. G_c was determined from the slope of the impact energy U versus $BD\phi$, where B is the width and D is the thickness of the specimen and ϕ is a geometrical function of the ratio between initial crack length, a, and the specimen thickness, D, i.e. a/D [19]. Standard deviation of this measurement is approximately 10%. Values of CNIS, measured for a constant $a/D = 0.3$, are averaged from ten specimens and the standard deviation was approximately 10%.

Fracture surfaces for morphological observations were prepared by breaking rectangular bars of the material containing a sharp razor blade notch in liquid nitrogen and then etching for 1–5 min in boiling n-heptane to remove the elastomer. Longer etching time had to be used when the elastomer encapsulated the filler, because the chemically bonded elastomer possesses significantly greater resistance to the etching. Fracture surfaces of specimens broken during impact tests and etched under the same conditions as above were used for observations of failure mechanisms. A thin layer of gold was deposited prior to observations in the scanning electron microscope (SEM) Amray IV (Amray, USA).

3. Results and discussion

3.1. Complete separation and strong adhesion

3.1.1. Effect of phase geometry ([MPP/EPR]/filler = [60/10]/30)

The increase in the content of maleic anhydride (MAH) in the matrix (MPP) enhances the separation of the filler and elastomer and, at the same time, strengthens matrix–filler adhesion. This process leads to an increase in both G_c and CNIS for ternary composites filled with both platelet-shaped $Mg(OH)_2$ and irregularly shaped, approximately spherical $CaCO_3$ particles (Fig. 1). In previous studies we have reported the effect of MAH concentration on the elastic modulus, tensile yield strength and morphology of this material and shown that complete separation of the elastomer and filler in the matrix is attained at concentrations equal to or greater than 1.5 wt % (based on filler content) [16, 17]. Because the grafting of MAH on to PP causes negligible reduction in its fracture toughness under the test conditions used [11], the trends observed for the ternary materials are attributed solely to the enhancement of matrix–filler adhesion and the change in composite morphology.

In order to distinguish the effect of improved adhesion from that of the dispersion of the filler in the matrix, one can relate G_c and CNIS of ternary [MPP/EPR]/filler composites to those of binary MPP/filler systems containing the same amounts of filler and MAH. The G_c values for the binary analogues of the systems shown in Fig. 1a are 1.1 kJ/m^{-2} ($CaCO_3$), 0.9 kJ m^{-2} ($Mg(OH)_2$ type A) and 0.7 kJ m^{-2} ($Mg(OH)_2$ type B). The ratio of strain energy release rates of the ternary composite relative to those of the binary analogues are thus 2.2 for $CaCO_3$, 2.2 for $Mg(OH)_2$ type A and 2.7 for the $Mg(OH)_2$ type B filled materials, respectively. The values of CNIS for the binary systems containing 30 vol % filler and 1.5 wt % MAH are 2.4 kJ m^{-2} ($CaCO_3$), 1.8 kJ m^{-2} ($Mg(OH)_2$ type A) and 1.5 kJ m^{-2} ($Mg(OH)_2$ type B), yielding corresponding ratios of CNIS of 1.5, 1.4 and 1.6, respectively. This suggests a substantial effect of the dispersed elastomer on the initiation values of fracture toughness and crack propagation in filled MPP.

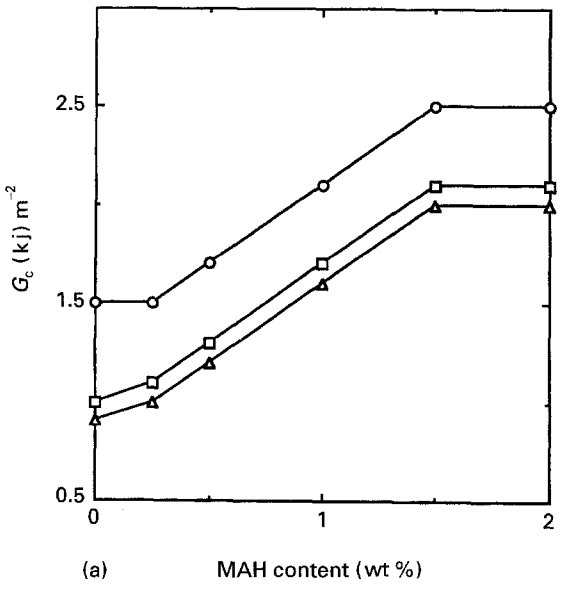

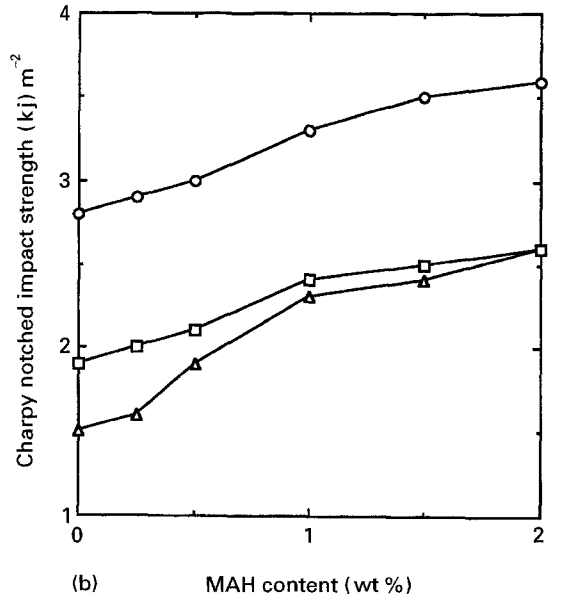

Figure 1(a) Dependence of the critical strain energy release rate, G_c, on the amount of maleic anhydride (MAH) in the matrix phase at constant composition of 30 and 10 vol % filler and elastomer, respectively. (b) Dependence of the Charpy notched impact strength (CNIS) on the amount of MAH in the matrix phase. (○) $CaCO_3$, (□) $Mg(OH)_2$ type A and (△) $Mg(OH)_2$ type B filled ternary composites.

3.1.2. Effect of the filler volume fraction at constant matrix composition ([MPP/EPR] = [60/10]) and 1.5 wt% MAH

The concentration dependence of G_c exhibits two distinct regions (Fig. 2). At $V_f < 0.055$, the materials fail by ductile tearing initiated around elastomer particles [20]. This failure process cannot be effectively described using the LEFM concept of localized yielding. The addition of a greater amount of rigid filler leads to a change of the failure mechanism from a ductile to a quasi-brittle one. Above $V_f = 0.055$, the LEFM concept of small-scale yielding can be used along with recognition of the mixed mode of failure [1, 2, 19, 21–25]. As was shown earlier [10], the material yield strength is the controlling variable determining the size of crack-tip plastic zones in plane stress (PSS) and plane strain (PSN) regions of the specimen. For the case of complete separation of the filler and elastomer and strong matrix–filler adhesion, the contributions to the measured fracture toughness from the PSS and PSN regions can be estimated using equations first proposed by Williams and co-workers [2, 21, 22], Ward *et al.* [22–25] and previously used by Jancar *et al.* [10, 11] for binary systems of PP and rigid fillers. Minimum values of the composite strain energy release rate, G_c', can be calculated using the expression

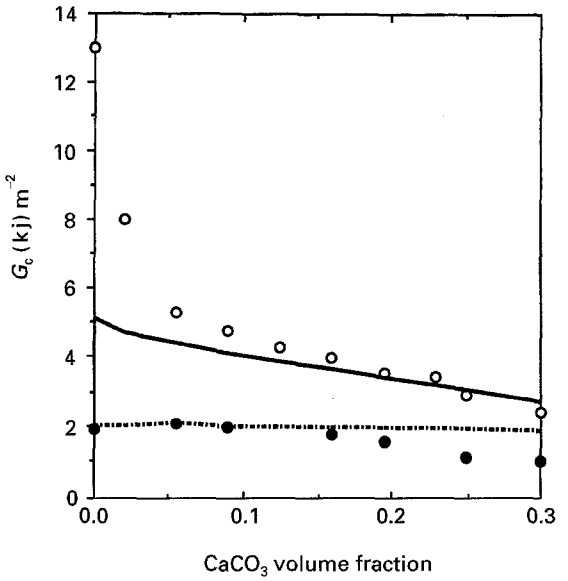

Figure 2 A comparison of the dependence of G_c on the $CaCO_3$ volume fraction for ternary [MPP/EPR]/$CaCO_3$ (○), [MPP/EPR] = 60/10 and (●) binary MPP/$CaCO_3$ composites at 1.5 wt % MAH (strong adhesion, complete separation) with the predicted limits (Equation 6).

$$(G_c')^{1/2} = \left(\frac{G_{1c}}{1-\nu^2}\right)^{1/2} + \frac{G_{2c}E}{\pi B\sigma_y^2} \times \left[G_{2c}^{1/2} - \left(\frac{G_{1c}}{1-\nu^2}\right)^{1/2}\right] \quad (1)$$

where G_{1c} and G_{2c} are critical strain energy release rates in plane strain and plane stress respectively, E is the elastic modulus, σ_y is the macroscopic yield strength and ν is Poisson's ratio of the composite and B is the thickness of the test specimen. Fig. 2 shows relatively good agreement between experimental and predicted behaviour. The data for the binary system were taken from the work of Jancar *et al.* [10]. The MPP matrix properties are shown in Table I (at an elastomer content $V_e = 0$). The specimen thickness was 0.004 m and the modulus and yield strength were measured at a strain rate of 2.6 m s^{-1}, matching the effective strain rate of the impact test. The effect of filler concentration on G_c' was determined by calculating the modulus, Poisson's ratio and yield strength of the composite from the following equations [26, 27]

$$\frac{E_c}{E_m} = \frac{(1 + ABV_f)}{1 - B\psi V_f} \quad (2a)$$

$$A = \frac{(7 - 5\nu_m)}{(8 - 10\nu_m)} \quad (2b)$$

$$B = \left(\frac{E_f}{E_m} - 1\right)\Big/\left(\frac{E_f}{E_m} + A\right) \quad (2c)$$

$$\psi = (1 + 0.89\nu_f) \quad (2d)$$

where the subscripts f and m refer to $CaCO_3$ and MPP, respectively

$$\frac{\sigma_{yc}}{\sigma_{ym}} = 1 + 0.33F(c)\nu_f^2 = 1 + 1.06\nu_f^2 \quad (3)$$

for $0.56 \geq V_f \geq 0$ and

$$\nu_c = \nu_f V_f + \nu_m(1 - V_f) \quad (4)$$

The Poisson's ratio and elastic modulus of the $CaCO_3$ filler are $\nu_f = 0.2$ and $E_f = 72$ GPa, respectively. Equation 1 appears to fit the experimental data up to a volume fraction of $CaCO_3$ of about 0.2. Above $\nu_f = 0.2$ the measured values for binary MPP/$CaCO_3$ binary composites are lower than those predicted as the effects of particle agglomeration become more noticeable.

The same process is used to calculate G_c' of the ternary blend, this time using the properties of a matrix containing 14 vol% EPR. i.e. [MPP/EPR] = 60/10. The properties of the new "quasi-homogeneous" binary matrix [MPP/EPR] = 60/10 can be calculated from the experimental values of G_c' for binary [MPP/EPR] blends using Equation 1 and the relation between G_{1c} and G_{2c} [19]

$$G_{2c} = \frac{G_{1c}}{(1 - 2\nu)^2} \quad (5)$$

Poisson's ratio is estimated from the simple rule of mixtures given by Equation 4, where the two constituents making up the matrix give $\nu_m = \nu_{EPR}V_{EPR} + \nu_{MPP}(1 - V_{EPR})$ with $\nu_{EPR} = 0.499$ and $\nu_{MPP} = 0.3$.

Combining Equations 1 and 5, one obtains a cubic equation in the variable $[G_{1c}/(1 - \nu^2)]^{1/2}$, containing one real and two imaginary roots, which can be solved for G_{1c}

$$G_c'^{1/2} = \left[\frac{G_{1c}}{(1 - \nu^2)}\right]^{1/2} + \left[\frac{G_{1c}}{(1 - \nu^2)}\right]^{3/2} \frac{E}{\pi B\sigma_y^2}\frac{(1 - \nu^2)}{(1 - 2\nu)^3} \times [(1 - \nu^2)^{1/2} - (1 - 2\nu)] \quad (6)$$

The elastic modulus of the binary matrix can be calculated from the Kerner–Nielsen equation, (Equation 2) and the yield strength from the Nicolais–Narkis equation [28]:

$$\frac{\sigma_{yc}}{\sigma_{yMPP}} = (1 - 1.21\nu_{EPR}^{2/3}) \quad (7)$$

The resulting values of G_{1c} and G_{2c} as a function of EPR content are shown in Table I. It is interesting to note that the calculated values of G_{1c} based on experimental data are independent of EPR content up to a concentration of about 10–15 vol% as assumed in previous publications [1, 2, 10, 11]. The predicted values for G_c' for the ternary blends based on [MPP/EPR] = 60/10 as a function of $CaCO_3$ concentration are then calculated as previously shown and represented by the solid line in Fig. 2.

3.1.3. Effect of EPR volume fraction at constant filler content (30 vol%) and MAH concentration (1.5 wt%)

In contrast to the previous case, the matrix properties are changing with increasing EPR volume fraction, while the rigid filler loading remains constant at 30 vol%. Equation 1 can be used to calculate the lower limit of G_c for different EPR volume fractions. The values of matrix critical strain energy release rate in plane strain, G_{1c}, and plane stress, G_{2c}, are again used together with the Kerner–Nielsen equation for composite modulus at $V_f = 0.3$ (Equation 2), the rule of mixtures for Poisson's ratio (Equation 4) and the appropriate equation for the yield strength for these materials [15, 27]

$$\sigma_{yc} = \sigma_{ym}[1 + 0.33F(c)\nu_f^2] \quad (8)$$

where $F(c) = 9.5$, 11.1 and 13.7 for the $CaCO_3$, $Mg(OH)_2$ type A and $Mg(OH)_2$ type B filled

TABLE I List of properties of binary blends MPP/EPR used to solve Equation 6 for G_{1c} from experimentally determined G_c' [11]. Values of G_{2c} were calculated from values G_{1c} and Poisson's ratio using Equation 5

EPR content V_{EPR}	Poisson's ratio, ν	Yield strength (MPa)	Elastic modulus (GPa)	Strain energy release rates	
				G_{1c}(kJ m^{-2})	G_{2c}(kJ m^{-2})
0	0.30	72.0	3.5	0.9	5.4
0.01	0.302	67.9	3.44	0.9	5.7
0.02	0.304	65.6	3.37	0.9	5.9
0.04	0.308	61.8	3.25	0.9	6.1
0.08	0.316	55.8	3.01	0.9	6.6
0.10	0.32	53.2	2.9	0.9	6.9
0.15	0.33	47.4	2.6	1.16	9.5
0.20	0.34	42.2	2.4	1.34[a]	13.7[a]
0.25	0.35	37.4	2.16	1.38[a]	14.4[a]
0.30	0.36	32.9	1.95	1.05[a]	13.4[a]

[a] Validity of the model limited.

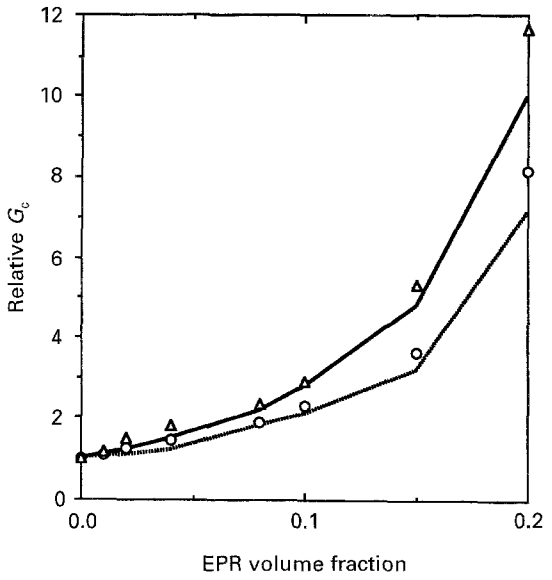

Figure 3 Dependence of the G_c of [MPP/EPR]/filler ternary composites relative to that of MPP/filler binary composites ($V_e = 0.0$) on the EPR volume fraction at 1.5 wt % MAH (per filler amount) in the matrix phase. Experimental data for (△) $Mg(OH)_2$ type B and (○) $CaCO_3$ filled composites. Lower limits calculated using Equations 2–4 and 6 for (——) $Mg(OH)_2$ type B and (···) $CaCO_3$ filled ternary composites ($V_f = 0.3$).

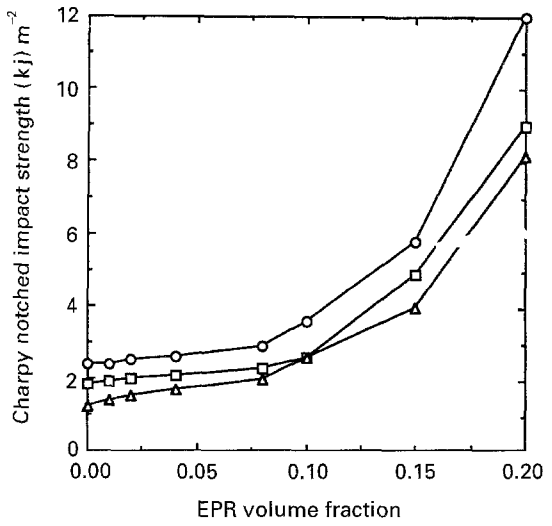

Figure 4 Concentration dependence of Charpy notched impact strength (CNIS) on the EPR volume fraction at 1.5 wt % MAH and $V_f = 0.3$. (○) $CaCO_3$, (□) $Mg(OH)_2$ type A and (△) $Mg(OH)_2$ type B filled ternary composites.

[MPP/EPR], respectively. The experimental data for G_c' for these materials are shown in Fig. 3 as a function of EPR concentration. Relatively good agreement is achieved between experimental data and calculated lower limit within the interval $0.1 > V_e > 0$. For EPR content greater than 10 vol %, the experimentally determined G_c' increases with elastomer content faster than predicted from Equation 1. Most probably, this is due to reductions in the yield strength which leads to development of plastic zones ahead of the crack tip too large to maintain the validity of the proposed LEFM model. The lower bound expresses in this case the most conservative values occurring in the case of brittle failure. Similar trends were observed also in the case of CNIS (Fig. 4).

3.2. Complete encapsulation/no adhesion

3.2.1. Effect of MAH content at constant composition (PP/[*MEPR/filler*] = *60/*[*10/30*])

Both strain energy release rate, G_c', and Charpy notched impact strength, CNIS, increased with increasing amount of MAH grafted on to EPR (Figs 5 and 6). The increasing amount of MAH leads to an enhancement of elastomer–filler adhesion, preventing the shear forces in the melt from separating the elastomer and filler inclusions in the course of melt mixing. At an MAH content in the elastomer (MEPR) of 1.5 wt % (based on rigid filler content), a plateau in the strain energy release rate is reached and the morphology is characterized by complete encapsulation of the filler by the elastomer. Because there is virtually no adhesion between the core–shell inclusions of [filler/MEPR] and PP matrix, one may compare the fracture toughness of PP/[MEPR/filler] ternary composites to that of the binary PP/filler composites of the same filler content in order to assess the effect of the MEPR. In PP/[MEPR/filler] composites, the volume fraction of core–shell inclusions in the sum of MEPR and rigid filler contents, i.e. $V_f^{tot} = V_e + 0.3$ ($V_e = 0.1$). The G_c' of these composites will be compared to those of PP/rigid filler composites of $V_f = 0.4$. At an MAH content of 1.5 wt % the G_c' of the binary blends with $CaCO_3$, $Mg(OH)_2$ type A and $Mg(OH)_2$ type B fillers are 0.7, 0.6 and 0.5 kJ m^{-2}, respectively. The corresponding ratios G_c^{ter}/G_c^{bin} are 5.4, 4.8 and 5.2, respectively. The presence of the soft interphase enhances significantly the strain energy release rate in these particulate composites by moderating the stress concentrations at interfaces and by further reducing matrix–filler adhesion. The enhancement of the resistance against crack propagation, as expressed in terms of CNIS, is also significant, as expressed by corresponding ratios $(CNIS)^{ter}/(CNIS)^{bin}$ of 4.0, 3.1 and 3.9, respectively.

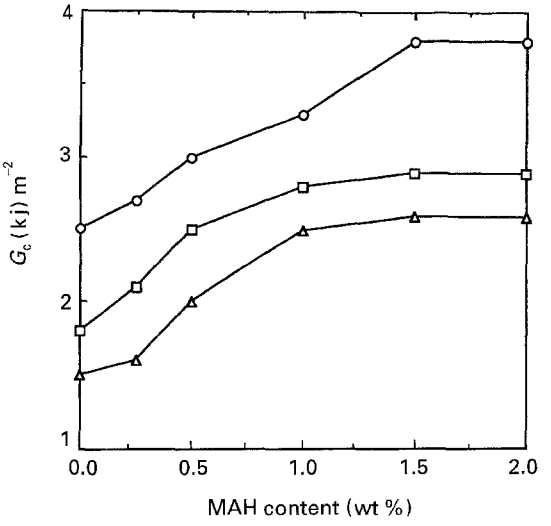

Figure 5 Dependence of the critical strain energy release rate G_c on the amount of maleic anhydride (MAH) in the elastomer phase at constant composition of 30 and 10 vol % filler and elastomer, respectively. (○) $CaCO_3$, (□) $Mg(OH)_2$ type A and (△) $Mg(OH)_2$ type B filled ternary composites.

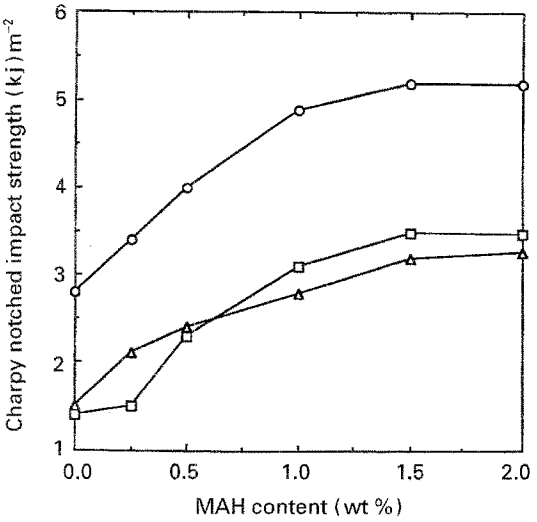

Figure 6 Dependence of the Charpy notched impact strength (CNIS) on the amount of MAH in the elastomer phase. For key, see Fig. 5.

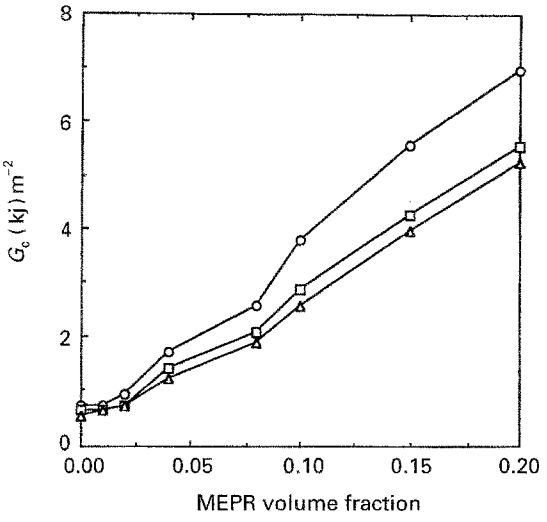

Figure 7 Dependence of G_c of PP/[MEPR/filler] ternary composites on the MEPR volume fraction at 1.5 wt % MAH (per filler amount) in the elastomer phase. For key, see Fig. 5.

3.2.2. Effect of MEPR volume fraction at constant filler and MAH contents (30 vol % rigid filler, 1.5 wt % MAH)

A significant increase in G_c is observed with increasing MEPR volume fraction (Fig. 7). At elastomer content greater than $V_e = 0.08$, the G_c for the PP/[MEPR/filler] ternary composites exceeds that of neat PP. Optical examination of fracture surfaces indicates that it is reasonable to assume that at 1.5 wt % MAH content there is nearly complete encapsulation of the rigid particles by the MEPR and no adhesion between matrix and core–shell inclusions. Thus, one can use the concepts of Irwin plastic zone size [18] at the crack tip and mixed mode of fracture [1, 10, 11, 19, 21–25] to calculate G_c as a function of MEPR volume fraction. An upper limit of the strain energy release rate can be calculated using Equations 1, 2 and 4–6 to calculate values of G_{1c}, G_{2c}, E and ν_m for the neat PP and its composites in the same manner as decribed in the previous sections of this paper. The concentration dependence of the yield strength is obtained using the results described by Equation 7a in Part I of this work [17]. A summary of calculated values for these properties is given in Table II. Relatively good agreement is achieved between the experimental data and calculated upper limiting values of G_c (Fig. 8). The higher yield strength of $Mg(OH)_2$-filled materials results in a smaller plastic zone and, thus, lower values of G_c' than those of $CaCO_3$-filled composites. Similar trends are also observed for the crack propagation as expressed in terms of CNIS (Fig. 9).

To evaluate the effect of elastomer layer on the fracture toughness of these materials, one can compare G_c and CNIS for binary PP/$CaCO_3$ and PP/$Mg(OH)_2$ composites with those for ternary PP/[MEPR/$CaCO_3$] and PP/[MEPR/$Mg(OH)]_2$ materials at the same inclusion volume fractions (Figs 10 and 11). The addition of rigid filler above $V_f = 0.3$ to the binary PP/rigid filler composites caused reduction in both G_c and CNIS. This may be attributed to agglomeration of filler particles causing material to fail in a brittle manner [10]. On the other hand, the addition of MEPR instead of rigid filler results in significant increase in both G_c' and CNIS. Encapsulation of the filler particles by the MEPR changes the character of the inclusions from rigid to soft and, importantly, limits the extent of agglomeration, changing the failure mechanism from quasi-brittle to ductile tearing.

TABLE II List of material parameters used to calculate G_c' of ternary composites using Equation 6. Poisson's ratios were calculated using rule of mixtures (Equation 4) and elastic modulus was calculated using the Kerner–Nielsen equation (Equation 2)

Filler content V_{CaCO_3}	Poisson's ratio, ν	Yield strength (MPa)	Elastic modulus (GPa)	Strain energy release rate, G_c' (kJ m^{-2})
0	0.33	47.5	2.6	5.1
0.025	0.325	47.6	2.7	4.7
0.05	0.322	48.0	2.9	4.6
0.075	0.319	48.5	3.0	4.5
0.10	0.316	49.0	3.1	4.1
0.125	0.313	49.8	3.3	3.9
0.15	0.309	51.5	3.6	3.7
0.19	0.304	53.2	4.1	3.6
0.21	0.301	54.8	4.2	3.4
0.25	0.295	56.8	4.7	3.1
0.30	0.291	63.4	5.4	2.8

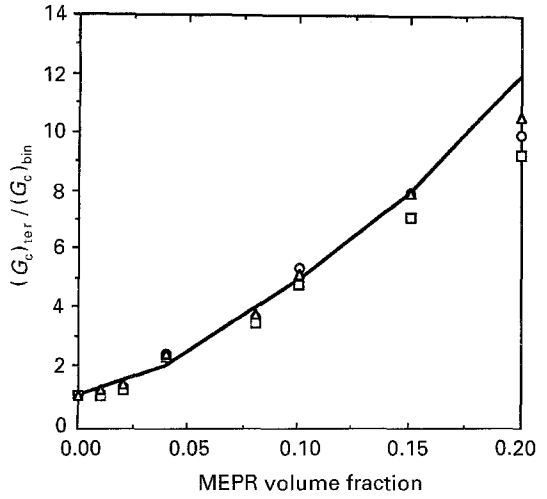

Figure 8 Dependence of G_c of PP/[MEPR/filler] ternary composites relative to that of PP/filler binary composites ($V_e = 0.0$) on the MEPR volume fraction at 1.5 wt % MAH (per filler amount) in the elastomer phase. For key, see Fig. 5. Upper limit calculated using Equation 6 and assuming core–shell inclusions action as elastomer particles.

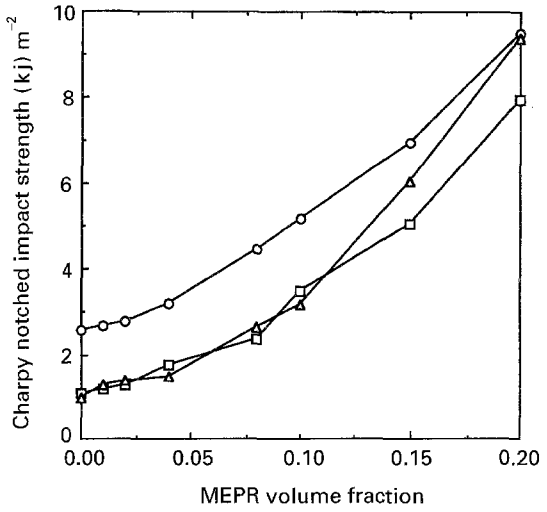

Figure 9 Concentration dependence of Charpy notched impact strength (CNIS) on the MEPR volume fraction at 1.5 wt % MAH and $V_f = 0.3$. For key, see Fig. 5.

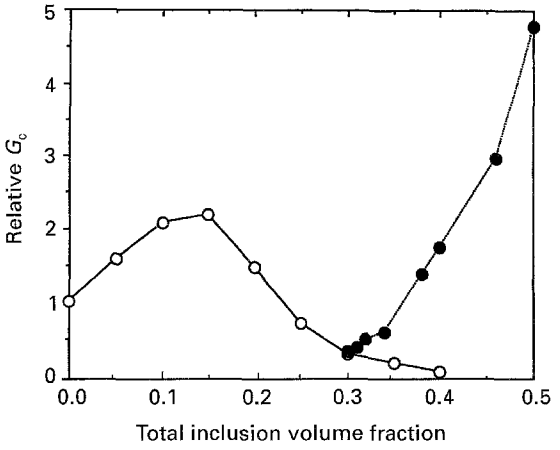

Figure 10 A comparison of the dependence of G_c of composites relative to that of neat PP on the total volume fraction of inclusions (no adhesion, complete encapsulation). (○) PP/$CaCO_3$ binary composites, (●) ternary composites of PP/[MEPR/$CaCO_3$] with 1.5 wt % MAH in the elastomer phase and 30 vol % rigid filler.

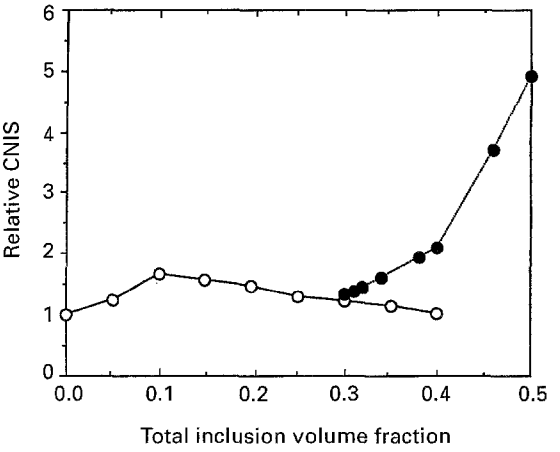

Figure 11 A comparison of the dependence of CNIS of composites relative to that of neat PP on the total volume fraction of inclusions (no adhesion, complete encapsulation). (○) PP/$CaCO_3$ binary composites, (●) ternary composites of PP/[MEPR/$CaCO_3$] with 1.5 wt % MAH in the elastomer phase and 30 vol % rigid filler.

4. Conclusion

The analysis described above demonstrates the dominant role of yield strength in the fracture of ternary composites of polypropylene filled with inorganic fillers and elastomer inclusions. It has been shown that the presence of the elastomer, as either particles dispersed uniformly in the MPP matrix phase or as interlayers on the rigid filler surfaces, enhances both strain energy release rate and resistance against crack propagation. LEFM and the Irwin concept of localized yielding along with our proposed model for yielding in ternary composites provided a satisfactory framework for the prediction of upper and lower limits of G_c for the two limiting morphologies of complete encapsulation of the rigid fillers by elastomer, and the complete separation and dispersion of rigid filler and elastomer in the polypropylene matrix.

The enhancement of matrix–filler adhesion by means of maleated PP (MPP) generates a morphology that is close to the idealized model of complete separation and perfect adhesion. This maximizes the material yield strength and stiffness and results in the lower limit of both G_c and CNIS. The enhancement of filler–elastomer adhesion generates a morphology that is close to the upper limiting case of complete encapsulation and no adhesion between core–shell inclusions and PP matrix. The mechanical response of this composite is similar to that of a ductile matrix filled with voids, thereby minimizing the yield strength and stiffness, which results in an upper limit for both G_c and CNIS.

Our laboratory work shows that a range of materials exhibiting mechanical behaviour between the upper and lower bounds can be generated by the appropriate choice of processing conditions, filler size, shape and concentration, elastomer content and the distribution of adhesion promoter between the phases.

References

1. J. M. HODGKINSON, A. SAVADORI and J. G. WILLIAMS, *J. Mater. Sci.* **18** (1983) 2319.

2. P. L. FERNANDO and J. G. WILLIAMS, *Polym. Eng. Sci.* **20** (1980) 215.
3. S. WU, *Polymer* **26** (1985) 1855.
4. *Idem, J. Appl. Polym. Sci.* **35** (1988) 549.
5. R. J. M. BORGGREVE, *Polymer* **28** (1987) 1489.
6. R. J. M. BORGGREVE, R. J. GAYMANS and A. R. LUTTMER, *Makromol. Chem. Macromol. Symp.* **16** (1988) 195.
7. B. Z. JANG, D. R. UHLMANN and J. B. VANDER SANDE, *J. Appl. Polym. Sci.* **29** (1984) 3409.
8. *Idem, ibid.* **29** (1984) 4377.
9. *Idem, ibid.* **30** (1985) 2485.
10. J. JANCAR, A. DiANSELMO and A. T. DiBENEDETTO, *Polym. Eng. Sci.* **33** (1993) 559.
11. J. JANCAR, A. DIANSELMO, A. T. DIBENEDETTO and J. KUCERA, *J. Polymer* **34** (1993) 1684.
12. J. KOLARIK, F. LEDNICKY, J. JANCAR and B. PUKANSZKY, *Polym. Commun.* **30** (1991) 201.
13. J. KOLARIK, F. LEDNICKY and B. PUKANSZKY, in "Proceedings of the 6th International Conference on Composite Materials" Edited by F. L. Mathews, N. C. R. Bushell, J. M. Hodgkinson and J. Mordon. (Elsevier, London, 1987) p. 452.
14. W.-Y. CHIANG, W.-D. YANG and B. PUKANSZKY, *Polym. Eng. Sci.* **32** (1992) 641.
15. J. JANCAR and A. T. DiBENEDETTO, in "Proceedings of the 51st ANTEC SPE", Brookfield New Orleans, 9–12 May 1993, p. 1698.
16. *Idem*, in "Proceedings of the 24th IUPAC Symposium on Macromolecules", Prague, 12–18 July 1993 (VSP Publishers) p. 399.
17. *Idem, J. Mater. Sci.* **28** (1993) 0000.
18. F. A. McCLINTOCK and G. R. IRWIN, "Fracture Toughness Testing" (ASM, Philadelphia 1965) p. 85.
19. J. WILLIAMS, "Fracture Mechanics of Polymers" (Ellis Horwood, Chichester, 1983) p. 100.
20. A. J. KINLOCK and R. J. YOUNG, "Fracture Behavior of Polymers" (Elsevier, London, 1983) Ch. 6, p. 182.
21. M. PARVIN and J. G. WILLIAMS, *J. Mater. Sci.* **10** (1975) 1883.
22. *Idem, Int. J. Fract.* **11** (1975) 963.
23. R. A. FRASER and I. M. WARD, *Polymer* **19** (1978) 220.
24. G. L. PITMAN and I. M. WARD, *ibid.* **20** (1979) 895.
25. P. J. HINE, R. A. DUCKETT and I. M. WARD, *ibid.* **22** (1981) 1745.
26. L. E. NIELSEN, "Mechanical Properties of Polymers and Composites", Vol. 11 (Dekker New York, 1974) p. 387.
27. J. JANCAR, A. DiANSELMO and A. T. DiBENEDETTO, *Polym. Eng. Sci.* **32** (1992) 1394.
28. L. NICOLAIS and M. NARKIS, *ibid.* **11** (1971) 194.

Received 23 June 1993
and accepted 8 September 1994